Dynamic mechanisms of generation of oscillatory cluster patterns in a globally coupled chemical system

.

NJIT CAMS Technical Report 1112-10

Horacio G. Rotstein[a)] and Hui Wu

Department of Mathematical Sciences, New Jersey Institute of Technology, Newark, NJ 07102

(Dated: 20 August 2012)

We use simulations and dynamical systems tools to investigate the mechanisms of generation of phase-locked and localized oscillatory cluster patterns in a globally coupled Oregonator model where the activator receives global feedback from the inhibitor, mimicking experimental results observed in the photosensitive Belousov-Zhabotinsky reaction. A homogeneous two-cluster system (two clusters with equal cluster size) displays antiphase patterns. Heterogenous two-cluster systems (two clusters with different sizes) display both phase-locked and localized patterns depending on the parameter values. In a localized pattern the oscillation amplitude of the largest cluster is roughly an order of magnitude smaller than the oscillation amplitude of the smaller cluster, reflecting the effect of self-inhibition exerted by the global feedback term. The transition from phase-locked to localized cluster patterns occurs as the intensity of global feedback increases. Three qualitatively different basic mechanisms, described previously for a globally coupled FitzHugh-Nagumo model, are involved in the generation of the observed patterns. The swing-and-release mechanism is related to the canard phenomenon (canard explosion of limit cycles) in relaxation oscillators. The hold-and-release and hold-and-escape mechanisms are related to the release and escape mechanisms in synaptically connected neural models. The methods we use can be extended to the investigation of oscillatory chemical reactions with other types of non-local coupling.

PACS numbers: 05.45.-a, 47.20.Ky, 82.20.-w, 82.40.Bj

[a)]Also at Center for Applied Mathematics and Statistics, New Jersey Institute of Technology.; Electronic

mail: horacio@njit.edu.

I. INTRODUCTION

The Belousov-Zhabotinsky (BZ) reaction is the prototypical example of nonlinear chemical oscillations[1–7]. It consists of the oxidation of malonic acid by bromate ions (BrO_3^-) in an acid medium, and catalyzed by cerium (Ce)[8]. Sustained periodic relaxation oscillations are observed in the concentrations of the catalyst's two ionization states: Ce^{3+} and Ce^{4+}. These oscillations are reflected in the periodic change of color of the solution from yellow (Ce^{4+}) to colorless (Ce^{3+}). When ferroin ($[Fe(phen)_3^{2+}]$)[9], instead of Ce, is used as catalyst, the dominating colors are red and blue[10].

Oscillatory cluster patterns have been recently discovered in the BZ reaction with photochemical global feedback (global coupling)[11,12] which is imposed through illumination in the photosensitive BZ reaction using the photosensitive catalyst Rubipy ($Ru(bipy)_3^{2+}$)[13]. The average concentration of Rubipy, taken over the working area of the gel, was employed to control the intensity of actinic light in such a way that the global feedback input is negative[11,12].

Oscillatory clusters are sets of oscillators, or domains, in which nearly all elements in a given domain oscillate with the same amplitude and phase[14–18]. The three most relevant cluster patterns observed in the globally coupled BZ reaction are two-phase, three-phase and localized clusters[11]. The former two consist of two or three clusters oscillating synchronously out-of-phase. The latter consists of two out-of-phase clusters in one region of the reactor while the remaining cluster shows no oscillations or oscillations with a very small amplitude (an order of magnitude smaller)[11,17,19]. Clusters with the same amplitude and phase need not be physically connected[11].

The Oregonator[20] is the simplest, chemically plausible mathematical model for the BZ reaction. It is an activator/inhibitor system with nonlinearities arising from the rate equations of mass kinetics. It was derived as a reduced version of the Fields-Koros-Noyes (FKN) mechanism[20] by applying quasi-steady-state and rate-limiting-step approximations. Chemical oscillations arise in the Oregonator for the appropriate parameter values[1,21–23] as the result of the interplay between an autocatalytic step and a feedback loop. A modified version of the Oregonator has been proposed in[24] to model certain dynamic behavior not captured by the "classical" Oregonator. Caricature models such as the FitzHugh-Nagumo (FHN) model[25,26] have also been used to capture dynamic aspects of the BZ reaction and other

excitable and oscillatory chemical and biological systems[2,27].

Simulations using both the Oregonator and the modified Oregonator proposed in[24] with global coupling reproduce the experimental results on cluster patterns mentioned above[11,19]. The dynamic mechanisms that govern the generation of phase-locked cluster patterns in the Oregonator and their transition to localized patterns are still not understood.

In this paper we use simulations and dynamical systems tools to investigate the dynamic mechanisms of generation of phase-locked two-cluster patterns and their transition to localized (two-cluster) patterns in a globally coupled Oregonator with a global feedback term similar to the one used in[12,17,19]. We use a self-consistent argument by assuming the existence of two separate clusters, initially oscillating out of phase, and investigate under what circumstances the system evolves into a two-cluster solution and, if the two-cluster structure is indeed maintained (that is, if the two clusters do not synchronize in phase), how do the steady phase (defined more precisely below) and amplitudes of the oscillations depend on the cluster size and other model parameters.

In previous work[16], we have investigated the mechanism of generation of localized clusters in a modified version of the FitzHugh-Nagumo (FHN) model with global coupling. More recently, we have investigated the mechanism of generation of phase locked clusters in a globally coupled FHN model[18] (see also the accompanying Technical Report in[28]). FHN type models serve as caricature models of excitable and oscillatory systems but they lack the complexity of the more realistic, chemically plausible Oregonator. In particular, the global coupling term in the FHN models investigated in[16,18] is linear while the global coupling term in the Oregonator is nonlinear and includes a chemical parameter responsible for this nonlinearity. The additional complexity of the Oregonator translates into more complex oscillatory patterns under the effects of global coupling. Most notably, the globally coupled Oregonator displays localized oscillatory patterns. Specifically, for two clusters with different sizes, the globally coupled FHN model supports M:1 patterns consisting of M large amplitude oscillation of the largest cluster per cycle (that is, per large amplitude oscillation of the smallest cluster) while the Oregonator supports M:1 localized oscillations where the largest cluster displays M small amplitude oscillations per cycle.

In our investigation of the globally coupled FHN model[18] (see also[28]) we have identified three qualitatively different basic mechanisms that are involved in the generation of phase-locked patterns: *swing-and-release*, *hold-and-release*, and *hold-and-escape*. The *swing-*

and-release mechanism is related to the canard phenomenon[29,30]. The *hold-and-release* and *hold-and-escape* mechanisms are related to the release and escape mechanisms in synaptically connected neural models[31–33]. We refer the reader to these references[18,28] for a detailed explanation of these mechanisms. Here, we show that they are also involved in the generation of phase-locked and localized clusters patterns in the more complex globally coupled Oregonator, and explain how they operate and the specific roles they play in the generation of these patterns.

In this paper we disregard spatial structure and we focus on the mechanism by which clusters with different phases, amplitudes, or both are generated. The mechanism by which oscillators within a cluster group into spatially extended domains will be investigated elsewhere.

In Section II, we first describe the globally coupled Oregonator we use in this paper. Then, we provide a short overview of the canard phenomenon. Finally, we describe the two-cluster simplification that allows a reduction of a large system of globally coupled oscillators into a system of two globally coupled oscillators representing two clusters. This cluster simplification is similar to the ones we used in[16–18]. In Section III, we discuss the various patterns observed in the globally coupled Oregonator. In Section IV, we explain the dynamic mechanisms that give rise to phase-locked patterns in homogeneous systems where the two clusters have the same cluster size. In Section V, we explain the mechanisms that give rise to phase-locked and localized patterns in heterogeneous systems where the two clusters have different sizes. Localized cluster patterns do not arise in homogeneous systems. We discuss our results in Section VI.

II. MODELS AND BACKGROUND

A. Oregonator model

The dimensionless kinetic equations are given by[21,34]

$$\begin{cases} \epsilon\ dx/dt = q\,y - x\,y + x\,(1-x), \\ \sigma\ dy/dt = -q\,y - x\,y + \eta\,z, \\ \quad dz/dt = x - z \end{cases} \tag{1}$$

where the three dimensionless variables x, y and z are normalized concentrations of $HBrO_2$,

Br^- and the oxidized form of the catalyst respectively. The dimensionless parameters ϵ, σ and q contain information about the rate equations of the five irreversible steps of the reduced mechanism and the concentrations of malonic acid. Typical values are $\sigma \ll \epsilon \ll 1$ and $q \ll 1$. The parameter η is a stoichiometric factor that serves as an adjustable parameter. A further reduction is possible by noting that $\sigma \ll q \ll \epsilon$, yielding

$$y = \frac{\eta\, z}{q + x}. \tag{2}$$

Substitution into (1) yields

$$\begin{cases} \epsilon\; dx/dt = x\,(1 - x) + \eta\;(q - x)/(q + x)\;z, \\ \quad dz/dt = x - z. \end{cases} \tag{3}$$

In the literature, x is usually referred to as the activator and z as the inhibitor. After a change of variables, $\hat{z} = \eta\, z$, and a rescaling of time, $\hat{t} = t/\epsilon$, the parameters η and ϵ move to the second equation yielding

$$\begin{cases} dx/dt = x\,(1 - x) + (q - x)/(q + x)\;z, \\ dz/dt = \epsilon\,(\eta\; x - z). \end{cases} \tag{4}$$

where for simplicity we have dropped the "hat" from the variables z and t; i.e., $\hat{z} \to z$ and $\hat{t} \to t$.

In Fig. 1-A we illustrate the dynamics of system (4) in the oscillatory regime for a representative set of parameters ($\eta = 1$, $q = 0.01$ and $\epsilon = 0.025$). Since $\epsilon \ll 1$, system (4) is fast-slow and oscillations are of relaxation type, evolving fast (jump up and jump down) in between a "silent" and "active" phases. In Fig. 1-C we show the phase-plane for the variables x and z which includes the x- and z-nullclines

$$N_z(x) = \eta\, x \qquad \text{and} \qquad N_x(x) = \frac{x\;(1 - x)\;(x + q)}{x - q} \tag{5}$$

and the limit cycle trajectory corresponding to the oscillations in Fig. 1-A. The x- and z-nullclines (Fig. 1-B) are the set of points in the (x, z)-plane for which $dx/dt = 0$ and $dz/dt = 0$ respectively. The x-nullcline is cubic-like. The left and right branches are stable and the middle branch is unstable. The two-nullclines intersect at the unstable fixed point $(\bar{x}, \bar{z})$ located in the middle branch. Phase-planes provide a description of the system dynamics in terms of the system's geometric properties but they do not provide information

about the time evolution of the variables x and z. This information has to be inferred from their graphs as a function of t (panel A). The limit cycle trajectory evolves on a fast time scale when jumping up and down in between the "silent" and "active" branches, and evolves on a slower time scale along these two branches.

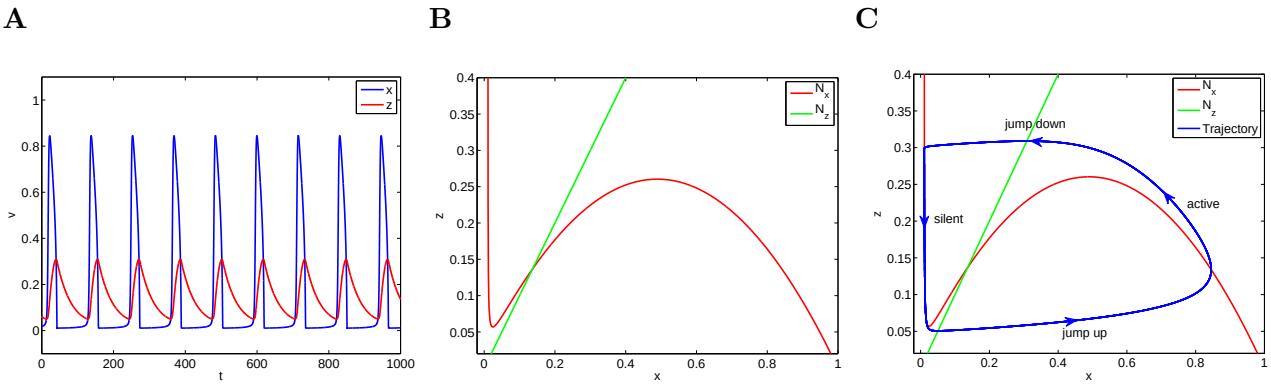

FIG. 1. **Dynamics of the uncoupled Oregonator for a representative set of parameter values.** **A.** Graphs of $x(t)$ and $z(t)$. **B.** Nullclines. **C.** Phase plane. We used the following parameter values: $q = 0.01$, $\eta = 1$ and $\epsilon = 0.025$.

B. Globally coupled Oregonator

Following the experimental setup for the globally coupled photosensitive BZ reaction, Oregonator models have been extended to include a term representing a global feedback from the inhibitor (z) to the activator (x)[11,17,19] of the form

$$\gamma \left(< z > - z_{tgt} \right) \frac{q - x}{q + x} \tag{6}$$

where $< z >$ represents the instantaneous spatial average of the activator z, and z_{tgt} represents the target value of the inhibitor (oxidized form of the catalyst) which, following others[19], was set equal to the unstable steady state concentration (unstable fixed-point) $\bar{z}$. The global feedback parameter γ depends on the maximum actinic light intensity and on the quantum yield of the photochemical reaction[11,19]. For a discrete system of N oscillators (indexed by $k = 1, \ldots, N$),

$$< z >= \frac{1}{N} \sum_{k=1}^{N} z_k. \tag{7}$$

The resulting globally coupled Oregonator model is given by

$$\begin{cases} dx/dt = x\,(1-x) + [\,z + \gamma\,(< z > - z_{tgt})\,]\,(q-x)/(q+x), \\ dz/dt = \epsilon\,(\eta\,x - z). \end{cases} \tag{8}$$

In this system, the activator is receiving global information from the inhibitor. In addition, since $q < x$ for most values of x ($q \ll 1$), this effect is mostly inhibitory in the sense that it is "negative". In general, there is a difference between global inhibition and the global effect of an inhibitor variables. Inhibition refers to the "negative" effect of either an activator or inhibitor variable. When $\gamma > 0$, system (8) is globally inhibited through the inhibitor variable. We used a similar type of global coupling (although linear) in the FitzHugh-Nagumo model investigated in[18] (see also[28]). In the FHN model studied in[35,36], on the other hand, the activator received global inhibitory feedback through the activator variable.

C. The canard phenomenon

The canard phenomenon (canard explosion) in two-dimensional oscillators of relaxation type refers to the abrupt increase in the amplitude of the limit cycle created in a Hopf bifurcation as a control parameter crosses a very small critical range[29,30,37–41]. Depending on whether the Hopf bifurcation is supercritical or subcritical, the small amplitude limit cycles are either stable or unstable respectively. The large amplitude, relaxation-type limit cycles are always stable. In system (4), the control parameter is η and the critical range is exponentially small in ϵ which is the parameter measuring the time scale separation between the activator (x) and the inhibitor (z). The Hopf bifurcation occurs as the fixed-point transitions from the left (stable) to the middle (unstable) branches of the cubic-like x-nullcline.

In Fig. 2 we illustrate the canard phenomenon for system (4) with $\epsilon = 0.025$ as η changes between $\eta = 2.2358$ (SAOs) and $\eta = 2.2357$ (LAOs). Note that as η decreases, the fixed-point $(\bar{x}, \bar{z})$ of system (4) moves further away from the minimum of the cubic-like nullcline (see Appendix A). Note also that the frequency for SAOs is larger than for LAOs.

A salient feature of the canard phenomenon, relevant to the mechanism we describe here, is that trajectories are able to evolve in close vicinities of the unstable (middle) branch of the cubic-like nullcline for a significant amount of time before moving either to the left, to generate SAOs, or to the right, to generate LAOs (see Fig. 2, right panels). This behavior occurs for values of the control parameter η close to its critical range (panels A and B). For larger values of η (larger distances between the fixed-point and the minimum of the cubic-like nullcline), once limit cycle trajectories reach a vicinity of the lower knee of the cubic-like nullcline (panel C), they move along the fast, horizontal, direction giving rise to fully developed relaxation oscillations.

The critical range of values of η over which the canard phenomenon occurs can be asymptotically approximated by a critical value η_{cr}[30]. We refer the reader to the Appendix in[42] for a technical discussion about the Hopf bifurcation and the canard phenomenon for two-dimensional systems. In Appendix A (of this paper) we provide an expression for η_{cr} in terms of the model parameters. We refer to the fixed-point corresponding to $\eta = \eta_{cr}$ as the critical fixed-point $(\bar{x}_{cr}, \bar{z}_{cr})$. Both $\bar{x}_{cr}$ and $\bar{z}_{cr}$ are monotonically decreasing functions of η_{cr}; i.e., as η_{cr} increases (decreases) the critical fixed-point moves to the left (right).

The canard phenomenon also occurs in higher dimensional models. In three-dimensional models[43] the canard phenomenon gives rise to mixed-mode oscillations[44,45] (patterns consisting of interspersed small and large amplitude oscillations). The canard phenomenon has been investigated in chemical systems[45–51]. In previous work, we have shown that the canard phenomenon plays an important role in the generation of localized solutions in a modified version of the Oregonator[17].

D. Two-cluster reduction

A *cluster* is a set of identical oscillators ("chemical points" of a reactor) that oscillate synchronously in-phase and with the same amplitude. A *two-cluster reduction* consists of assuming that a system of N globally coupled oscillators is divided into two clusters. All oscillators within a cluster oscillate synchronously (in phase) while different clusters may oscillate out-of-phase or display irregular patterns. Since all oscillators in a cluster are identical and have identical behavior, their dynamics can be described by the same set of equations. For a two-cluster system,

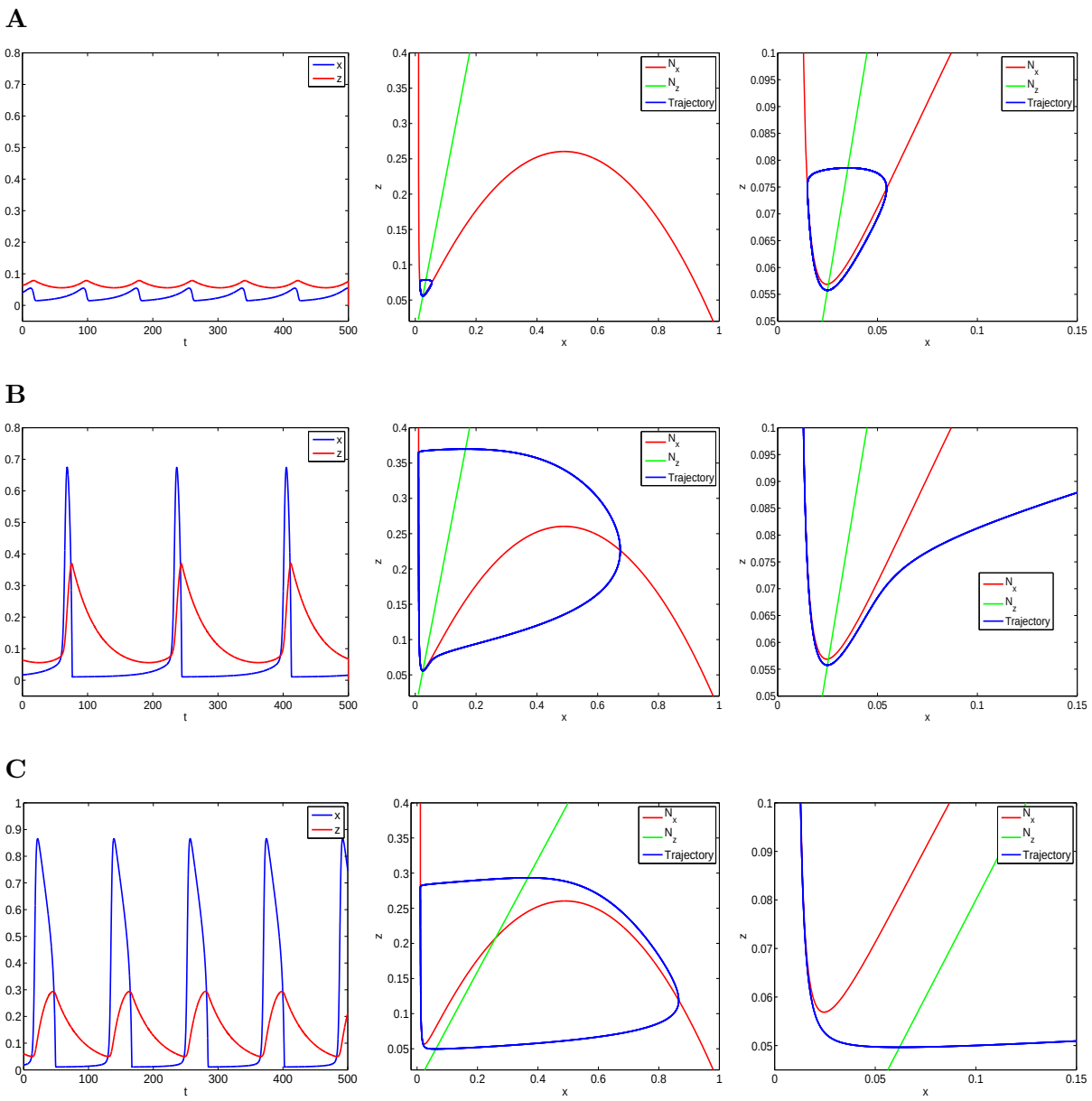

FIG. 2. **Supercritical canard phenomenon for the Oregonator for a representative set of parameters. A.** Small amplitude oscillations for $\eta = 2.2358$. **B.** Large amplitude oscillations for $\eta = 2.2357$. **C.** Large amplitude oscillations for $\eta = 0.8$. Left panels show the traces, middle panels show the phase-planes, and right panels show magnifications of the phase-planes around the lower knee. The canard critical value η_{cr} lies in between the values of η corresponding to panles A and B. We used the following parameters: $q = 0.01$ and $\epsilon = 0.025$. The curves N_x and N_z represent the x- and z-nullclines respectively.

$$< z >= \sigma_1 z_1 + \sigma_2 z_2 \tag{9}$$

with σ_k, $k = 1, 2$ representing the fraction of oscillators belonging to each cluster ($\sigma_1 + \sigma_2 = 1$). Substitution into (8) yields

$$\begin{cases} dx_k/dt = x_k\,(1 - x_k) + (q - x_k)/(q + x_k)\;[\,(1 + \gamma\,\sigma_k)\,z_k - \gamma\bar{z} + \gamma\,\sigma_j z_j\,] & k, j = 1, 2, \quad j \neq k \\ dz_k/dt = \epsilon\,(\eta\;x_k - z_k) & . \end{cases} \tag{10}$$

This is a system of two oscillators coupled through the inhibitor (z_1 and z_2). In Fig. 3 we illustrate the evolution of both the activator and inhibitor for a representative set of parameters. Initially (for values of t to the left of the vertical dashed-lines), the two oscillators were oscillating almost in phase. Their peaks separate soon after the global coupling is activated (vertical dashed-lines).

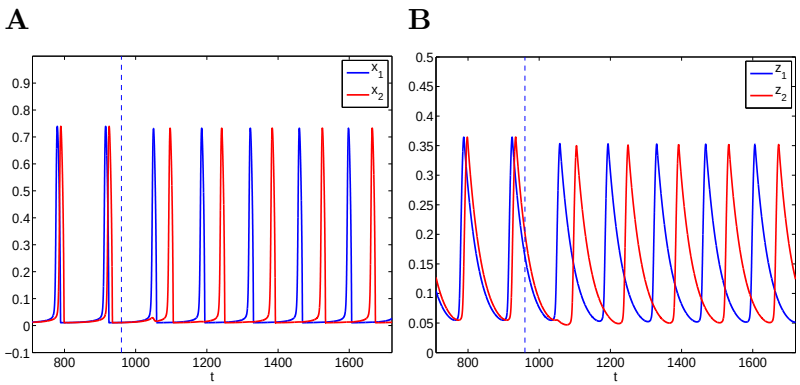

FIG. 3. **x- and z-traces for the globally coupled Oregonator model for a representative set of parameters.** The vertical dashed-lines indicate the time at which global coupling is activated. (For lower values of t the system is uncoupled.) We used the following parameters: $\eta = 2$, $\epsilon = 0.025$, $q = 0.01$, $\gamma = 0.1$, $\sigma_1 = 0.5$ and $\sigma_2 = 0.5$.

The zero-level surfaces ("higher-dimensional nullclines") for system (10) are given by

$$z_k = N_{x,k}(x_k, z_j) = \frac{x_k\;(1 - x_k)\;(x_k + q)}{(x_k - q)\,(1 + \gamma\,\sigma_k)} + \frac{\gamma\,z_{tgt}}{1 + \gamma\,\sigma_k} - \frac{\gamma\,\sigma_j\,z_j}{1 + \gamma\,\sigma_k} \qquad k, j = 1, 2,\;\; j \neq k \tag{11}$$

and $z_k = N_{z,k}(x_k) = \eta\,x_k$, $k = 1, 2$. Eq. (11) describes a two-dimensional surface having the shape of the first term $N_{z,k}(x_k, 0)$ in the right hand side in eq. (11). For $\gamma > 0$, the nullsurface

(11) can be thought of as the x-nullcline of the k^{th} oscillator for $\gamma = 0$, deformed (raised by an amount $\gamma\, z_{tgt}$ and flattened by the effect of the denominator), and forced by the second (j^{th}) oscillator via the function $z_j(t)$ ($j \neq k$). We refer to $N_{x,k}(x_k, 0)$ as the x_k-nullcline (or the autonomous part of the nullcline) and to the z_j-dependent term (last term) as the forcing term. The changes in the shape of this nullcline due to nonzero values of both σ_k and γ produce changes in the canard critical value $\eta_{cr}(\gamma, \sigma_k)$ ($k = 1, 2$) for the autonomous part of each oscillator in the globally coupled system. Oscillations in $z_j(t)$ "raise" and "lower" this x_k-nullcline. As a consequence, the intersection point with the (fixed) z_k-nullcline $N_z(x_k)$ "moves" describing a curve parametrized by t. Points in this curve are not fixed-points of the four dimensional system, but they play a significant role in organizing the dynamics of the coupled system. We refer to them as "effective fixed-points" (or just fixed-points). Since the curve of effective fixed-points is parametrized by t, as t progresses, the relative position between them and the minimum of the x-nullcline also changes. These changes have a transient effect on the resulting oscillations, in particular their amplitude regime.

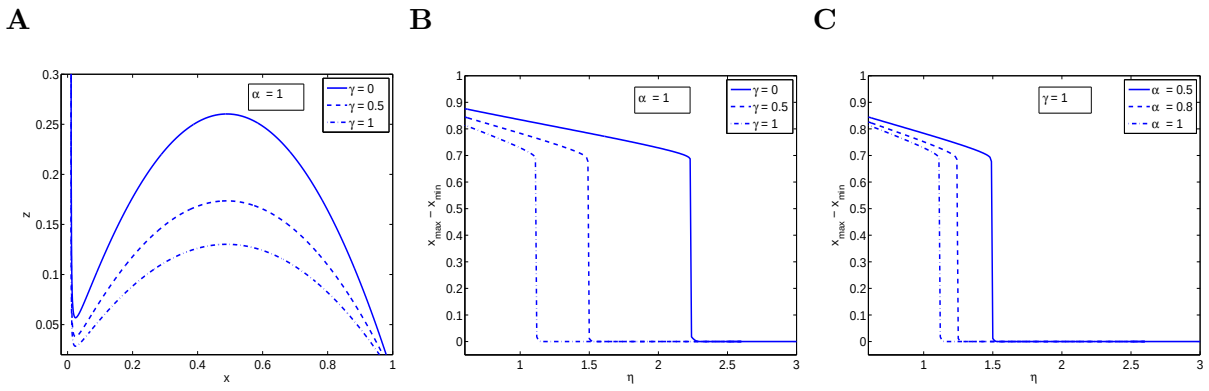

FIG. 4. **Effects of the global feedback parameter γ and the fraction α of oscillators in a cluster on the supercritical canard phenomenon for the Oregonator A.** x-nullclines for $\alpha = 1$ and various representative values of γ. **B.** Amplitude diagram for $\alpha = 1$ and various representative values of γ. **C.** Amplitude diagram for $\gamma = 1$ and various representative values of α.

In Fig. 4 we illustrate how changes in γ and the fraction α of oscillators in a given cluster affect the dynamics of the autonomous part ($z_j = 0$) of system (10). For simplicity we consider $z_{tgt} = 0$. Note that the parameter α corresponds to σ_k in eqs. (10) and (11). Fig. 4-A shows the x-nullclines (11) for various representative values of γ. As γ increases,

the middle and right branches of the x-nullcline become flatter and the lower knee becomes slightly wider. In Fig. 4-B we show the limit cycle amplitude diagrams (computed as $x_{max} - x_{min}$ as a function of η) for $\alpha = 1$ and various representative values of γ. As γ increases, $\eta_{cr}(\gamma)$ decreases. As a consequence, an abrupt transition from SAOs to LAOs may occur as the result of an increase in the value of γ. In Fig. 4-C we show the limit cycle amplitude diagrams for $\gamma = 1$ and various representative values of α. As expected, as α increases, η_{cr} decreases. As a consequence, two clusters with different sizes can display oscillations in different amplitude regimes (SAOs and LAOs) for a range of values of η. Since η parametrizes the fixed-point $(\bar{x}, \bar{z})$, these results can be stated in terms of fixed-point critical values: As γ increases, $\bar{x}_{cr}$ increases, and as α increases, $\bar{x}_{cr}$ increases. The forcing term may cause the effective fixed-points (parametrized by t) to move along both sides of the critical fixed-point thus transiently changing the limit cycle amplitude regime (from SAOs to LAOs and vice-versa). We previously made a similar observation for the modified Oregonator model studied in[16].

III. ANTIPHASE, OUT-OF-PHASE, AND IN-PHASE PATTERNS

In Fig. 3 we showed an example of an antiphase pattern for $\eta = 2$, $\gamma = 1$ and two clusters of equal size ($\sigma_1 = \sigma_2 = 0.5$). We define the phase difference between two oscillators (henceforth called "phase") as the absolute value of the time difference between two consecutive peaks in the graphs of $x_1(t)$ and $x_2(t)$ divided by their oscillation period (which is assumed to be the same for both oscillators). The phase for values of t prior to the connection time is equal to the initial phase. For antiphase oscillations, the phase is equal to 0.5.

In the example in Fig. 3, phase separation occurs very fast (in the first cycle). Both the final phase of two oscillators and the "pace" at which phase separation occurs depend on the parameter values and the initial conditions. We illustrate this dependence in Fig. 5. Panels A and B show the phase evolution from an initial phase (first few cycles where the two oscillators are still disconnected) to the steady phase for representative sets of values of the global feedback parameter ($\gamma = 0.1$ and $\gamma = 1$), stoichiometric factor ($\eta = 2$ and $\eta = 0.8$), and cluster sizes ($\sigma_1 = 0.5$ and $\sigma_1 = 0.2$) . For reference, in panel C we show the nullclines for the autonomous part of eq. (11) for $\gamma = 1$ and these values of σ_1 and η.

For $\sigma_1 = 0.5$, the two cubic-like x-nullclines are identical, and therefore their graphs are

superimposed. For $\sigma_1 = 0.2$, the red nullcline ($\sigma_2 = 0.8$) is flatter than the blue nullcline ($\sigma_1 = 0.2$). The z-nullclines are independent of γ but they depend on η. As η decreases, the slope of the z-nullcline also decreases, and the fixed-points move to the right. In both cases, the fixed-points are located in the middle (unstable) branch of the x-nullcline. For $\eta = 2$, the fixed-point is very close to the minimum of the x-nullcline, and for $\eta = 0.8$, the fixed-point is located roughly in the middle of the unstable branch.

For $\sigma_1 = 0.5$ and $\eta = 2$ (panel A_1), phase separation occurs very fast, and it occurs faster for larger values of γ. For $\gamma = 0.1$ (blue dots), there is bistability between in phase and antiphase patterns. The basin of attraction for in-phase patterns is much smaller than the basin of attraction for antiphase patterns. We have not observed in-phase patterns for $\gamma = 1$. If they exist, their basin of attraction is extremely small. For $\sigma_1 = 0.5$ and $\eta = 0.8$ (panel A_2), phase separation occurs at a slower pace than for $\eta = 2$. Bistability occurs for both values of γ with a larger basin of attraction for in-phase patterns for the lower value of γ (blue dots).

For $\sigma_1 = 0.2$ ($\sigma_2 = 0.8$), phase-locked patterns are no longer antiphase. Their phase depends on the value of γ. The behavior for $\eta = 2$ (panel B_1) is qualitatively similar to that in panel A_1. There is bistability for $\gamma = 0.1$ with a much smaller basin of attraction for in-phase patterns than for phase-locked patterns. Similarly to $\sigma_1 = 0.5$, we have not observed in-phase patterns for $\gamma = 1$. However, the behavior for $\eta = 0.8$ (panel B_2) is significantly different from that in the remaining panels. Most notably, there are not phase-locked patterns for both values of γ.

The differences among the various patterns are associated with differences among the corresponding nullclines (panel C) and can be explained using dynamical systems tools (phase-plane or phase-space analysis). Below we discuss the differences among the trajectories in phase-space corresponding to three qualitatively different patterns. In Section IV we discuss in more detail the dynamic mechanisms that give rise to these patterns.

In Figs. 6, 7 and 8 we show the x- and z-traces (panels A) for three sets of representative parameter values among these used in Fig. 5, and the trajectories in phase-space for both oscillators (panels B). More precisely, in panel B we show the projection of these trajectories onto the (x_1, z_1)- and (x_2, z_2)-planes respectively.

Figs. 6 ($\eta = 2$, $\gamma = 1$, and $\sigma_1 = 0.5$) corresponds to the red dots in Fig. 5-A_1. Initially, the two oscillators are disconnected and the phase is almost equal to zero with the blue

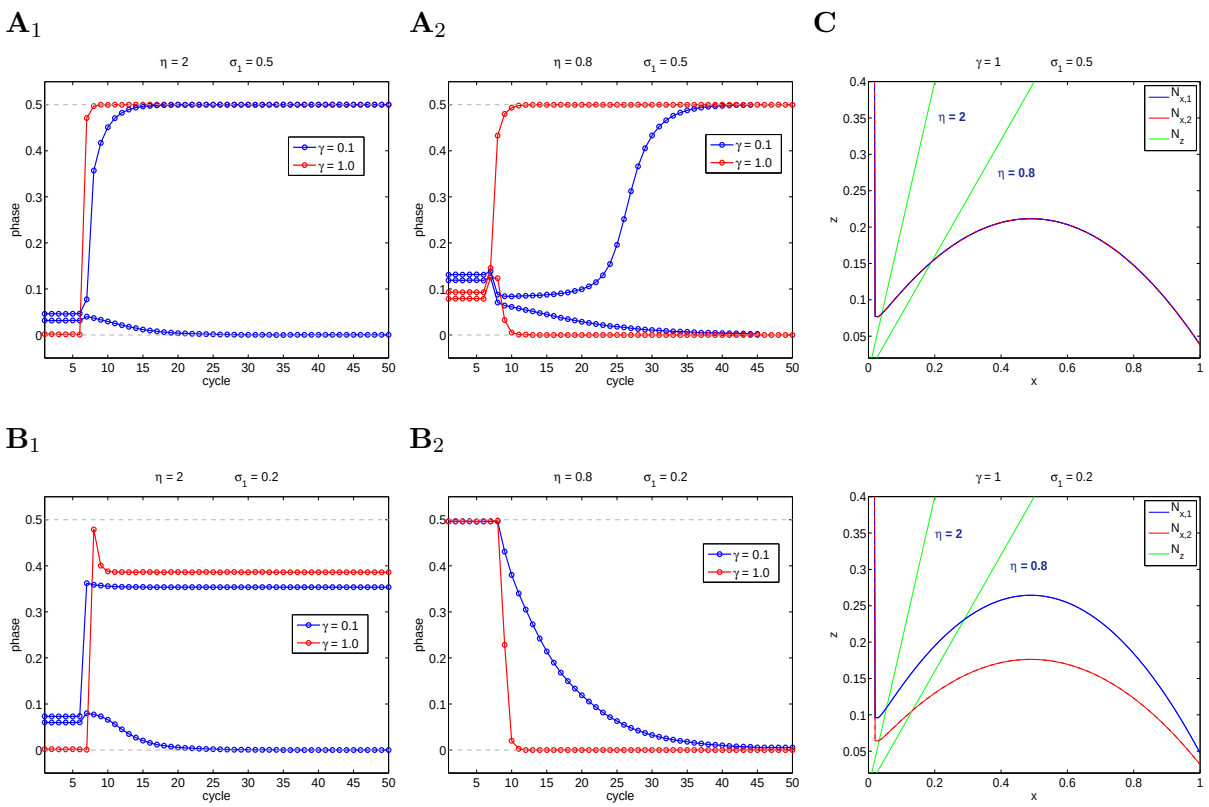

FIG. 5. **Phase evolution for the globally coupled Oregonator.** The two oscillators were connected after a few cycles. The phase for these cycles correspond to the initial phase. **A_1.** $\eta = 2$, $\sigma_1 = 0.5$ and $\sigma_2 = 0.5$. **A_2.** $\eta = 0.8$, $\sigma_1 = 0.5$ and $\sigma_2 = 0.5$. **B_1.** $\eta = 2$, $\sigma_1 = 0.2$ and $\sigma_2 = 0.8$. **B_2.** $\eta = 0.8$, $\sigma_1 = 0.2$ and $\sigma_2 = 0.8$. **C.** Phase planes for the autonomous part of the globally coupled Oregonator for $\gamma = 1$. In the top panel, the two cubic-like nullclines are identical, and therefore superimposed.

oscillator preceding the red oscillator. Phase separation occurs fast after global coupling is activated (vertical dashed-line). This fast phase separation is associated with a red SAO in the first cycle; that is, the blue oscillator inhibits the red oscillator which continues to be silent for a significant amount of time before peaking again. This is reflected as a loop (or "swing") in the red trajectory and a further decrease in its z_2 component. As we argue in Section IV, this mechanism is associated with the canard phenomenon described in Section II C. Canard-like SAOs are not observed in the blue oscillations nor in the subsequent red oscillations. A similar type of mechanism is observed for lower values of γ as we show in Fig. 8-A_1 for $\gamma = 0.1$ (blue dots in Fig. 5-A_1). Due to the lower value of γ, the canard-like SAO occurs in the second cycle after global coupling is activated instead of the first.

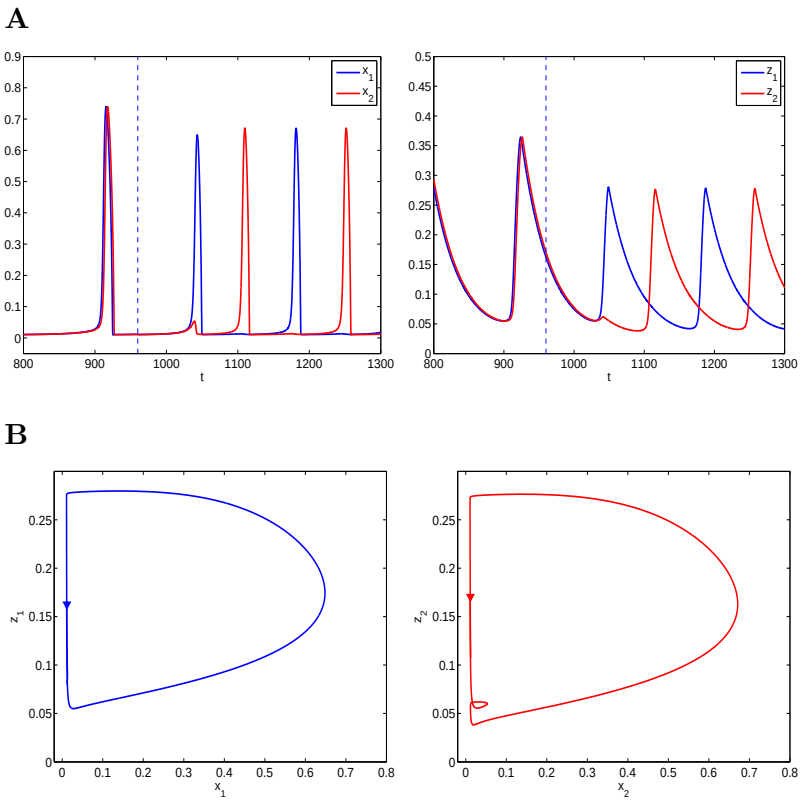

FIG. 6. **Dynamics of the globally coupled Oregonator model for a representative set of parameters. A.** x- and z-traces. The vertical dashed-lines indicate the time at which global coupling is activated. (For lower values of t the system is uncoupled.) **B.** Trajectories in phase-space projected onto the (x_1, z_1)-plane (left) (x_2, z_2)-plane (right) for the first cycle after global coupling is activated. The arrows indicate both the connection time and the direction of motion of the trajectory at the connection time. We used the following parameters: $\eta = 2$, $\epsilon = 0.025$, $q = 0.01$, $\gamma = 1$, $\alpha_1 = 0.5$ and $\alpha_2 = 0.5$.

In contrast to the case discussed in the previous paragraph, the transition from the initial phase to the antiphase pattern for $\gamma = 0.1$ in Fig. 5-A_2 (blue dots) occurs at a slower pace and does not involve a canard-like SAO as we show in Figs. 7 ($\eta = 0.8$, $\gamma = 0.1$, and $\sigma_1 = 0.5$). (We show only the first few cycles. The steady pattern is antiphase.) The phase separates slowly as the number of cycles progresses. The red oscillator is still inhibited by the blue oscillator, but the underlying structure of the vector field does not produce any initial SAO as part of the mechanism responsible for the fast phase separation. This behavior is in contrast to what we discussed above for $\gamma = 1$. One reason is that the z-nullcline is further away from the minimum of the cubic nullcline than in the previous case ($\eta = 2$, see Fig.

5-C, top panel).

The transition from an initial phase to the steady in-phase (zero-phase) patterns where the phase slowly decreases rather than increase as the number of cycles progresses is governed by a similar mechanism. In Figs. 8-A_1 and -A_2 ($\eta = 2$, $\gamma = 0.1$, and $\sigma_1 = 0.5$) we compare the first few cycles for the in-phase and antiphase patterns in Fig. 5-A_1 (blue dots). The initial phases in both panels A_1 and A_2 are very close (almost identical) but the phase separation occurs in the second cycle in panel A_1 (upper blue dots in Fig. 5-A_1) while it slowly decreases in panel A_2 (lower blue dots in Fig. 5-A_1).

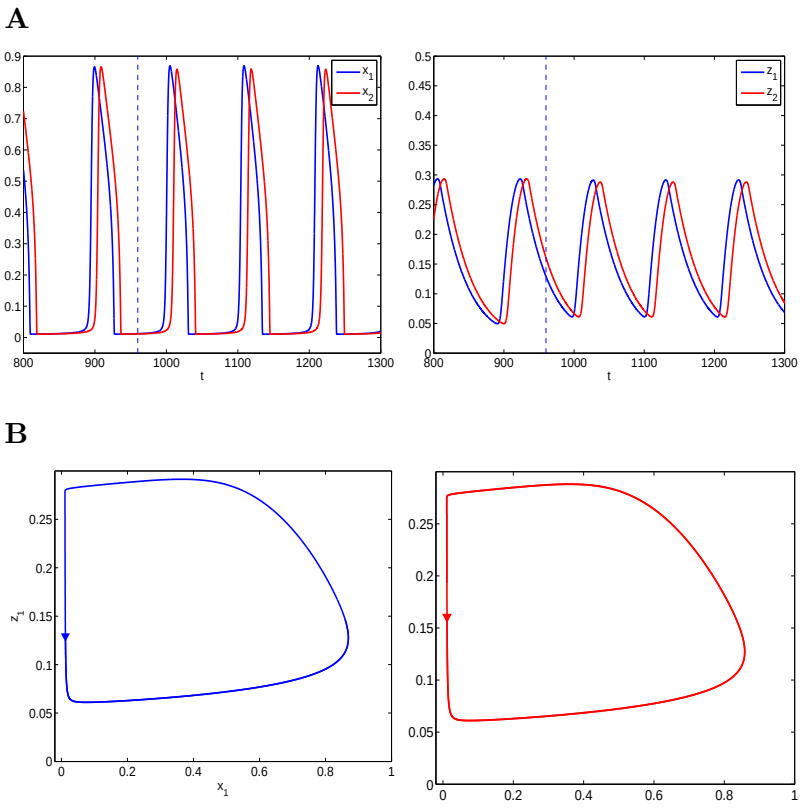

FIG. 7. **Dynamics of the globally coupled Oregonator model for a representative set of parameters. A.** x- and z-traces. The vertical dashed-lines indicate the time at which global coupling is activated. (For lower values of t the system is uncoupled.) **B.** Trajectories in phase-space projected onto the (x_1, z_1)-plane (left) (x_2, z_2)-plane (right) for the first cycle after global coupling is activated. The arrows indicate both the connection time and the direction of motion of the trajectory at the connection time. We used the following parameters: $\eta = 0.8$, $\epsilon = 0.025$, $q = 0.01$, $\gamma = 0.1$, $\alpha_1 = 0.5$ and $\alpha_2 = 0.5$.

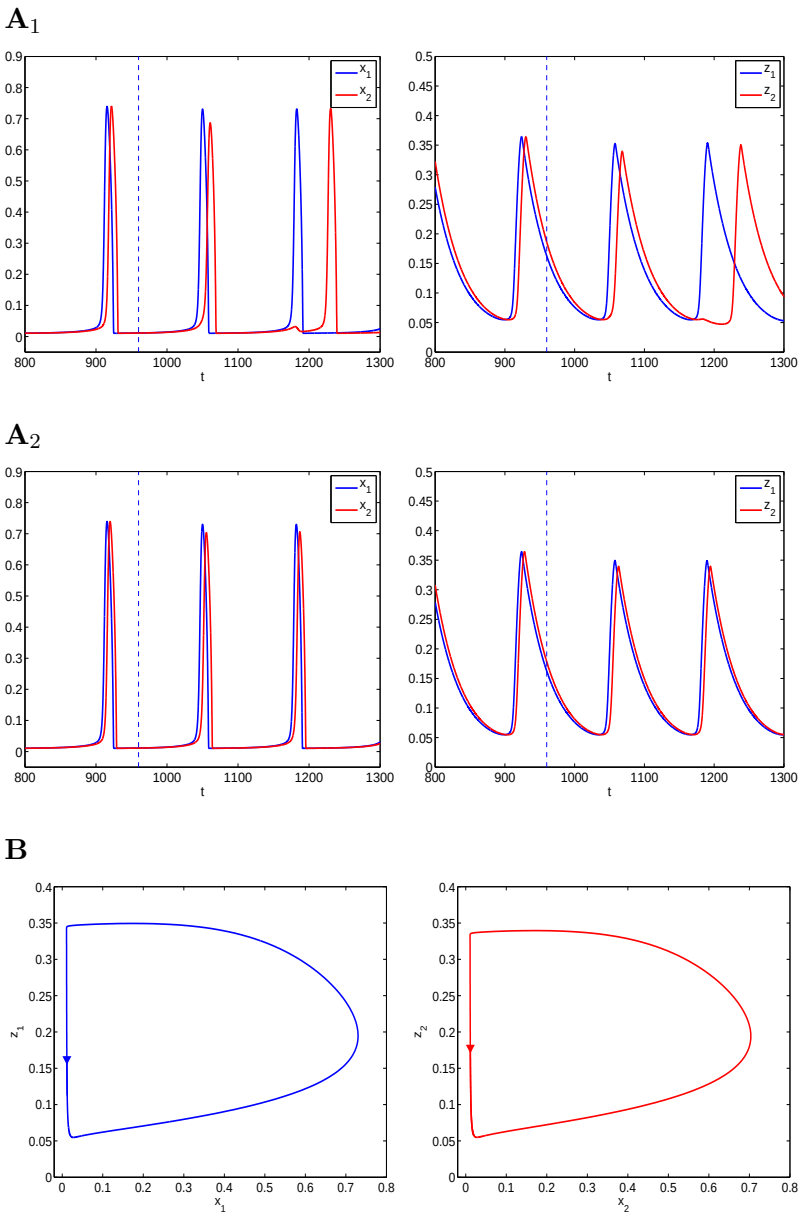

FIG. 8. **Dynamics of the globally coupled Oregonator model for a representative set of parameters. A.** x- and z-traces. The vertical dashed-lines indicate the time at which global coupling is activated. (For lower values of t the system is uncoupled.) **B.** Trajectories in phase-space projected onto the (x_1, z_1)-plane (left) (x_2, z_2)-plane (right) for the first cycle after global coupling is activated. The arrows indicate both the connection time and the direction of motion of the trajectory at the connection time. We used the following parameters: $\eta = 2$, $\epsilon = 0.025$, $q = 0.01$, $\gamma = 0.1$, $\alpha_1 = 0.5$ and $\alpha_2 = 0.5$.

IV. MECHANISMS OF GENERATION OF PHASE-LOCKED PATTERNS IN HOMOGENEOUS SYSTEMS

Here we use dynamical systems tools to investigate in more detail the mechanism of generation of antiphase patterns for the globally coupled Oregonator. We first consider the parameter values corresponding to Fig. 6 ($\eta = 2$, $\gamma = 1$, and $\sigma_1 = 0.5$) where a pattern with an initially small phase separates rapidly into an antiphase pattern (see Fig. 5-A_1, red dots). In Figs. 9 and Figs. 10 we show snapshots of superimposed phase-planes for various representative values of t along the first oscillation cycle after global coupling is activated. Panel A ($t = 0$) corresponds to the connection time in Fig. 6. The blue and red dots indicate the location of the tip of the trajectory at the corresponding time. The full trajectories are shown in Fig. 6-B.

Initially, the two oscillators are very close, therefore the corresponding cubic nullclines are almost superimposed. The blue nullcline is slightly lower than the red one because the red oscillator is "higher" than the blue one ($z_2 > z_1$). As time progresses, the two oscillators move along the cubic nullclines and approach each other. After they arrive to the lower knee (panels B), both oscillators start moving along the unstable branch of their cubic nullclines, slightly upwards (panels C), and separate from each other (panels D). Note that the blue oscillator moves faster than the red oscillator since it is further away along the fast direction of motion. As the blue oscillator moves upwards, z_1 increases slightly above z_2 and lowers the red nullcline (panels E) forcing the red oscillator to cross it (panels F) and reverse direction, moving towards the left branch, then crossing it again (panel G), and finally moving down along the left branch of the red nullcline. This creates the canard-like SAO observed in the Fig. 6. The amount of time the red oscillator spends moving around the knee of the red nullcline creates the necessary delay for the blue oscillator to "climb up" the blue nullcline, reach its upper knee, and jump down (panel H). The corresponding decrease in z_1 raises the red nullcline and releases the red oscillator from inhibition, thus allowing it to jump up (panels I and J). The accompanying increase in z_2 lowers the blue nullcline and holds the blue oscillator in the silent phase thus creating the necessary delay for the phase to be maintained; i.e., it provides the red oscillator with enough time to reach the upper knee of the red nullcline before the blue oscillator reaches the lower knee of the blue nullcline. After the red oscillator jumps down (panels K and L), the decrease in z_2 raises the blue

nullcline and releases the blue oscillator (panel M). Since the red oscillator is now further away from the blue one, the shifting down of the red nullcline after the blue oscillator jumps up again (not shown) holds the red oscillator but it does not create a canard-like SAO. For the parameters in this figure, phase separation occurs via a canard-related swing-and-release mechanism similar to the one described for the globally coupled FHN model in[18]. Critical to this mechanism is the fact that the fixed-point for the autonomous system is close enough to the minimum of the cubic-like nullclines. The antiphase pattern is maintained (stabilized) by a hold-and-release mechanism where the trajectory first moves down together with the nullcline, and then it is released when the nullcline moves back up.

In Fig. 11 we show snapshots of superimposed phase-planes for various representative values of t along an oscillation cycle for the parameters in Fig. 7. The full trajectories are shown in Fig. 7-B. Depending on the initial phase, the final pattern is either antiphase or in-phase (see Fig. 5-A_2, blue dots). Panel A ($t = 0$) corresponds to the connection time in Fig. 7. As time progresses, the two oscillators move down their cubic nullclines (panel B). After the blue oscillator reaches the lower knee of the blue nullcline, it jumps up (panel C). The corresponding increase in z_1 lowers the red nullcline. In contrast to the swing-and-release mechanisms described in before, the red oscillator jumps up (panels D-F) following the blue oscillator without being "caught" in a canard-like SAO. The main reason for this is the smaller value of η causes the fixed-point to be further away from the minimum of the cubic nullcline than in Figs. 10 and 10. Similar to Fig. 2-C, the underlying vector field causes the trajectory to leave the lower knee of the cubic nullcline along the fast (almost horizontal direction) instead of "climbing up" its middle branch. When the red nullcline moves down, it briefly holds the red oscillator, causing a small delay with respect to the blue oscillator. The occurrence of this delay depends on the initial distance between the two oscillators (initial phase). In other words, it depends on whether or not the red oscillator is able to jump up (escape inhibition) before the red nullcline move down a significant distance that is enough to hold it. If the delay is long enough, the phase will increase cycle by cycle, thus creating an antiphase pattern. Otherwise, the phase will contract on subsequent jumps. In the first case, the antiphase pattern is created by a hold-and-release mechanism similar to the one described in[18]. Note that the analysis presented here does not provide a quantitative measure of the boundary between the basins of attraction of the in-phase and antiphase patterns.

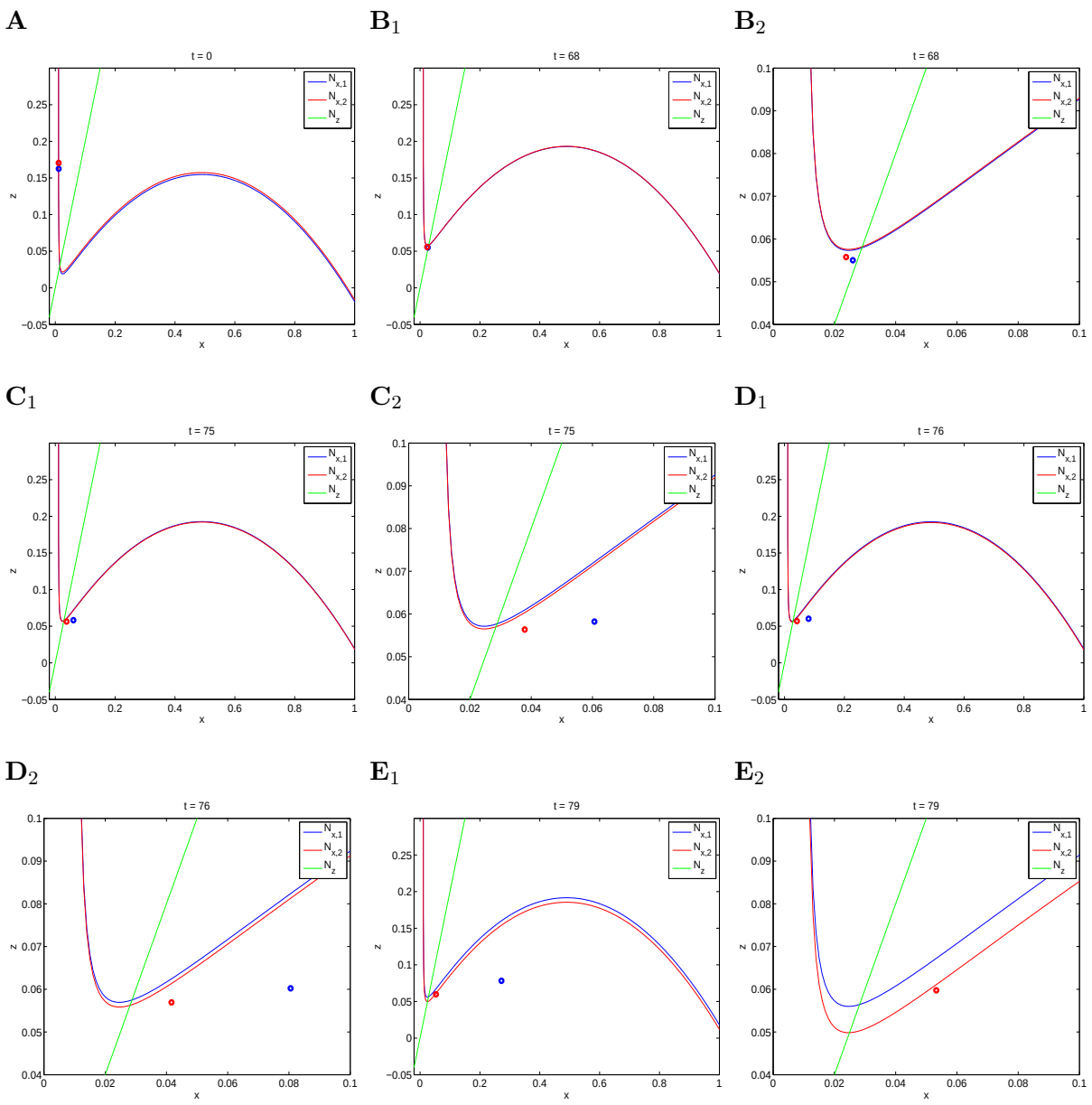

FIG. 9. **Globally coupled Oregonator (Part I).** Snapshots of the phase-plane for the two globally coupled oscillators for representative values of t. We used the following parameters: $\eta = 2$, $\epsilon = 0.025$, $q = 0.01$, $\gamma = 1$, $\alpha_1 = 0.5$ and $\alpha_2 = 0.5$. This figure continues in Fig. 10.

V. MECHANISMS OF GENERATION OF PHASE-LOCKED AND LOCALIZED PATTERNS IN HETEROGENEOUS SYSTEMS

Here we investigate the dynamics of the globally coupled Oregonator for two clusters having different sizes. In our simulations we used $\sigma_1 = 0.2$ and $\sigma_2 = 0.8$. Geometrically, the

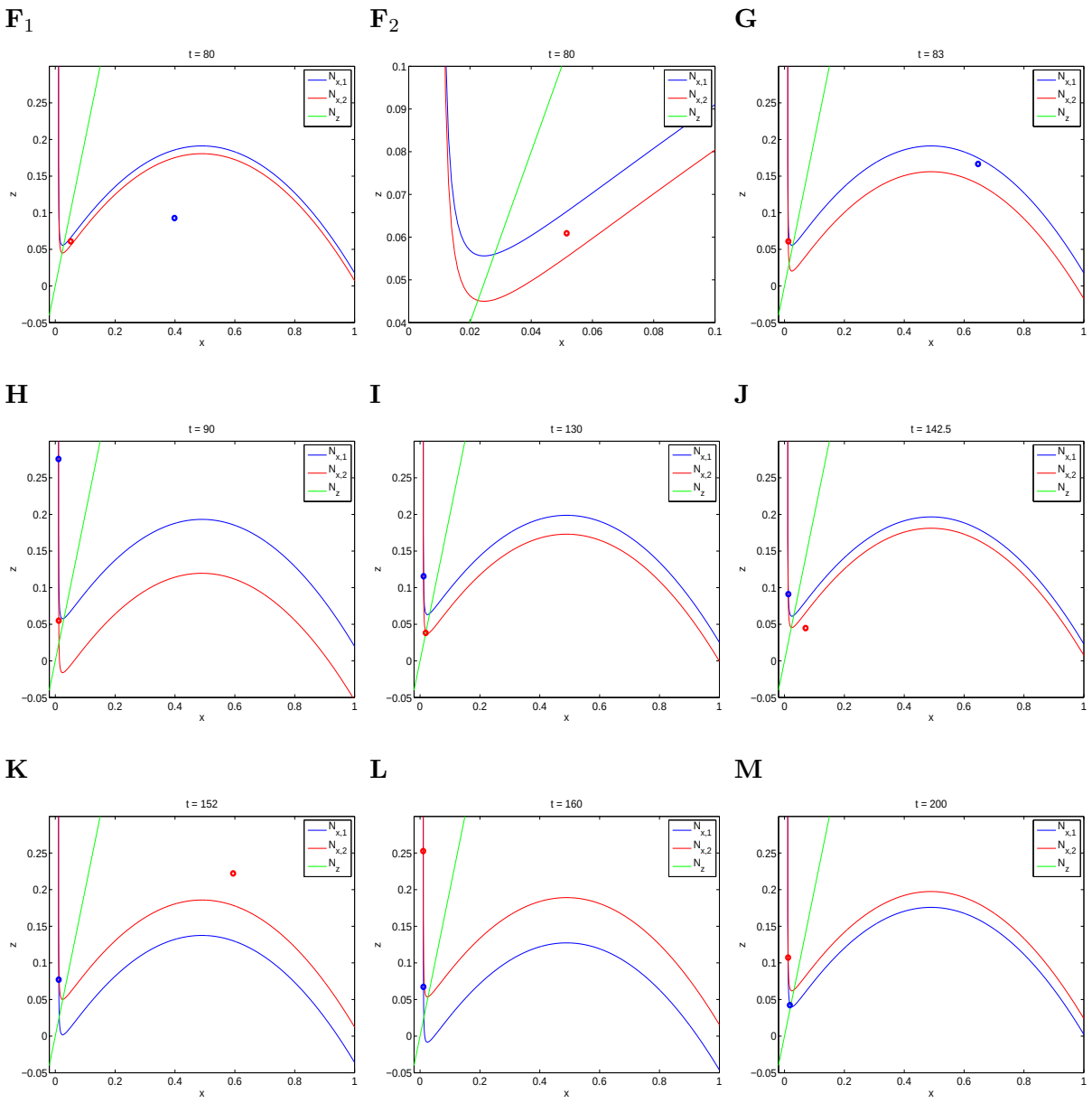

FIG. 10. **Globally coupled Oregonator (Part II).** Snapshots of the phase-plane for the two globally coupled oscillators for representative values of t. We used the following parameters: $\eta = 2$, $\epsilon = 0.025$, $q = 0.01$, $\gamma = 1$, $\alpha_1 = 0.5$ and $\alpha_2 = 0.5$. This figure is the continuation of Fig. 9.

effect of the different cluster sizes is reflected in the different shapes of the autonomous part of the nullclines in eq. (11). For a fixed value of γ, the larger the cluster size the flatter the nullcline since γ is multiplied by the cluster size in the denominator of the autonomous part in eq. (11). (This effect is similar to the one produced by γ in Fig. 4-A for a fixed value of the cluster size.) Dynamically, the effect of different cluster sizes is reflected in the forcing

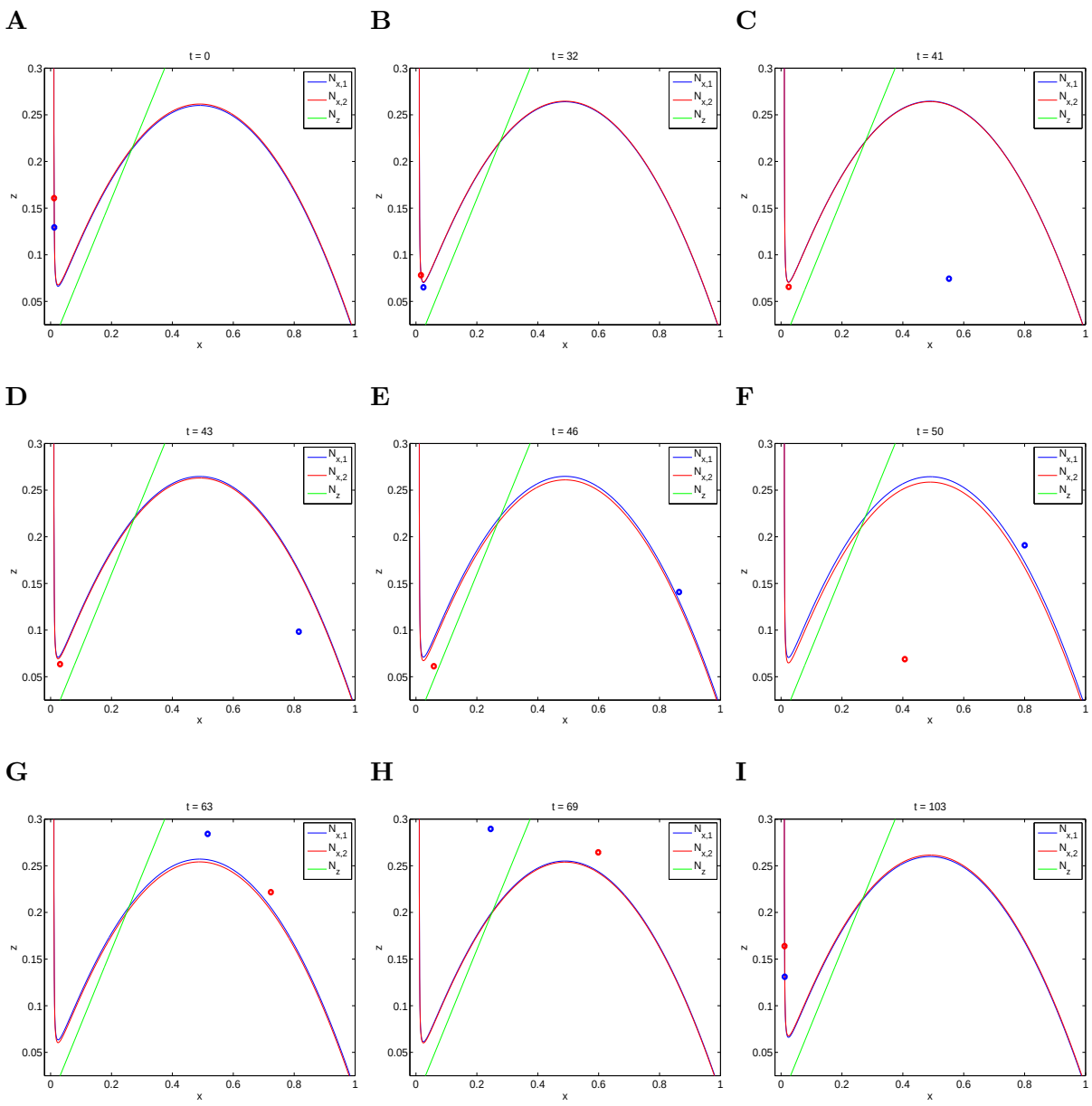

FIG. 11. **Globally coupled Oregonator.** Snapshots of the phase-plane for the two globally coupled oscillators for representative values of t. We used the following parameters: $\eta = 0.8$, $\epsilon = 0.025$, $q = 0.01$, $\gamma = 0.1$, $\alpha_1 = 0.5$ and $\alpha_2 = 0.5$.

term of the nullclines and the different canard critical values η_{cr} of their autonomous part (see Fig. 4). For a fixed value of γ, the larger the cluster size, the smaller η_{cr}. For a fixed value of γ, there is a range of values of η for which the autonomous part of oscillator with the largest cluster size is in the SAO regime while the autonomous part of the oscillator with the smallest cluster size is in the LAO regime. The forcing that each oscillator exerts

on the other may cause changes, at least transiently, in the oscillatory regime.

In Figs. 12, 13, and 14 we show the traces (panels A) and trajectories (panels B) for $\gamma = 1$, $\gamma = 3.5$, and $\gamma = 5$ respectively. In all these figures, the right panels B are magnifications of the left ones. The differences in the shapes of the nullclines caused by the two different values of σ_1 and σ_2 are reflected in the amplitude of the oscillations (panels A) and the corresponding sizes of the limit cycles (panels B).

In Fig. 12 ($\gamma = 1$), phase separation does not occur by a canard-like (swing-and-release) mechanism, as it occurs for $\sigma_1 = \sigma_2 = 0.5$, but by a hold-and-release mechanism where the red SAO is caused by the motion of the red nullcline. Specifically, the blue oscillator jumps up and lower the red nullcline before the red oscillator manages to jumps up. As a consequence its trajectory is slightly retracted and held for some time before it is released to jump up after the blue oscillator jumps down.

In Fig. 13 ($\gamma = 3.5$), the amplitude of the red oscillations (largest cluster size) is approximately half of the amplitude of the blue oscillations. Phase separation occurs via a mechanism similar to the one described for the parameters in Fig. 12. Red SAOs persist in all cycles. Note that the red LAOs are reminiscent of canard-like oscillations.

Fig. 14 ($\gamma = 5$) shows localized oscillations where the blue LAOs are approximately six times larger than the red, canard-like SAOs. The larger amplitude of these SAOs as compared to the canard-like SAOs in Fig. 3 is due to the fact that the red nullcline is flatter than the blue one (see Fig. 15). In Figs. 15 and 16 we show snapshots of superimposed phase-planes for various representative values of t along an oscillation cycle for the parameters in Fig. 14. At the beginning of the cycle (panel A) the two oscillators move down along the left branch of their corresponding nullclines. The red oscillator is located at a lower height than the blue oscillator. After the red oscillator reaches the lower knee (panel B) it is released (panel C), moves along the middle branch, and crosses it displaying a canard-like SAO (panels C, D, E). When the red oscillator arrives at the left branch of the red nullcline, it still has a lower height than the blue oscillator (panel E) that continues to move slowly down, behind the red oscillator. The red oscillator is released again describing a second canard-like SAO (panels F, G, H, I). This time, it arrives at the left branch at a higher height than the blue oscillator (panel J) . When the blue oscillator is released (panels K and L), it describes a LAO (panels M, N, O, P, Q), returning to the left nullcline at a higher height than the red oscillator (panel R). This completes the cycle. Critical to this mechanism

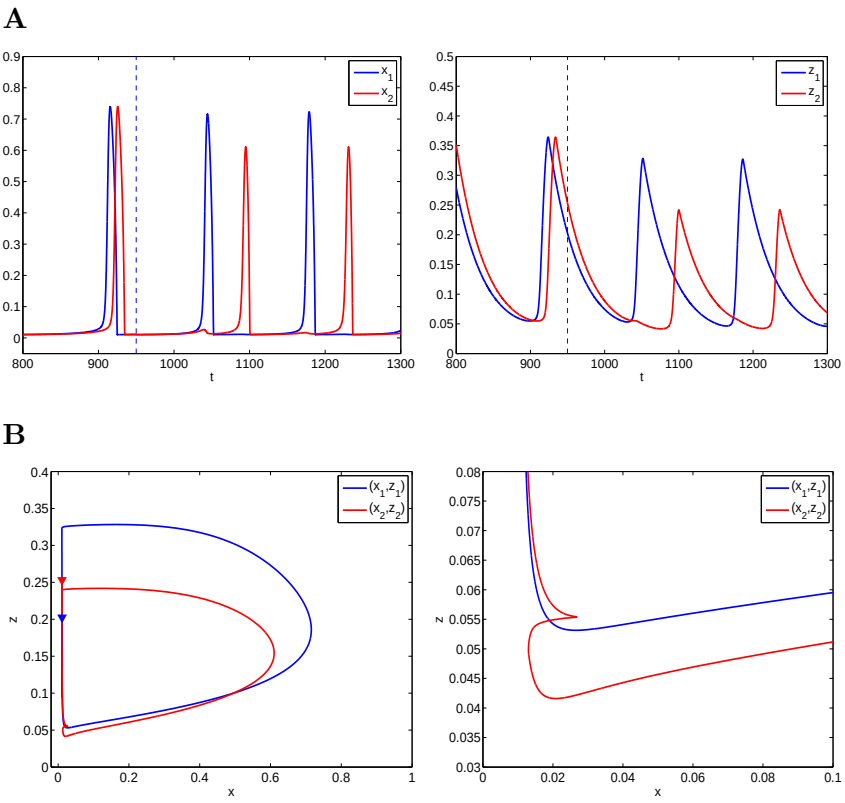

FIG. 12. **Dynamics of the globally coupled Oregonator model for a representative set of parameters. A.** x- and z-traces. The vertical dashed-lines indicate the time at which global coupling is activated. (For lower values of t the system is uncoupled.) **B.** Trajectories in phase-space projected onto the (x_1, z_1)-plane (left) (x_2, z_2)-plane (right). The arrows indicate both the connection time and the direction of motion of the trajectory at the connection time. We used the following parameters: $\eta = 2$, $\epsilon = 0.025$, $q = 0.01$, $\gamma = 1$, $\alpha_1 = 0.2$ and $\alpha_2 = 0.8$.

is the fact that the shapes of the red and blue nullclines determine the amplitude regime for the corresponding oscillations. In particular, the red oscillator displays only SAOs because its nullcline is flatter than the blue one.

VI. DISCUSSION

Phase-locked and localized oscillatory cluster patterns have been experimentally observed in the Belousov-Zhabotinsky (BZ) reaction with photochemical global feedback[11,12]. In these experiments, the average concentration of the inhibitor (photosensitive catalyst) was used

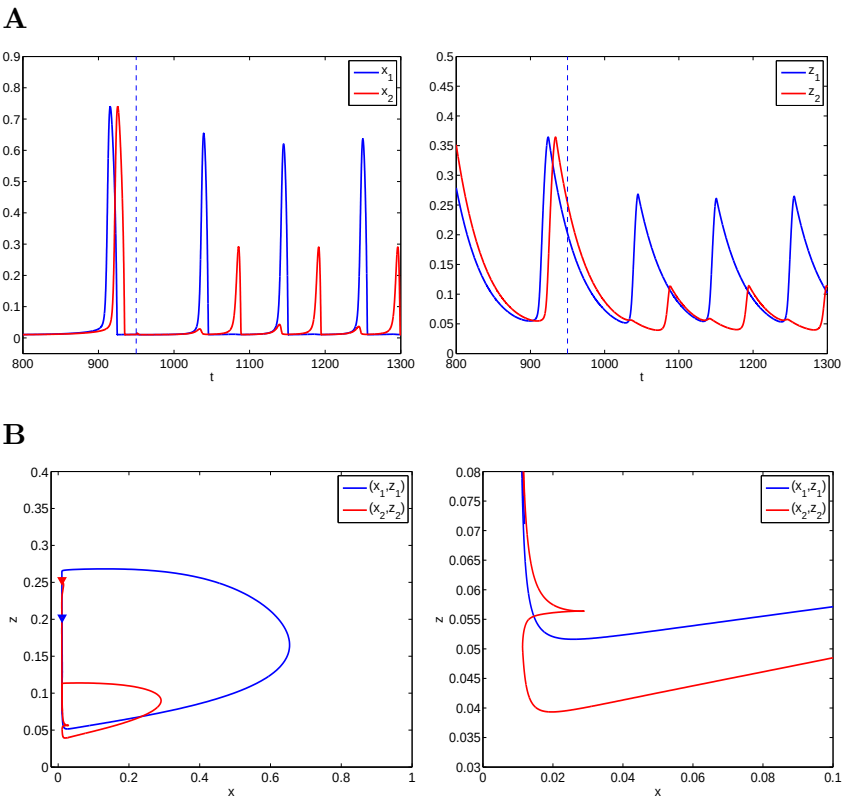

FIG. 13. **Dynamics of the globally coupled Oregonator model for a representative set of parameters. A.** x- and z-traces. The vertical dashed-lines indicate the time at which global coupling is activated. (For lower values of t the system is uncoupled.) **B.** Trajectories in phase-space projected onto the (x_1, z_1)-plane (left) (x_2, z_2)-plane (right). The arrows indicate both the connection time and the direction of motion of the trajectory at the connection time. We used the following parameters: $\eta = 2$, $\epsilon = 0.025$, $q = 0.01$, $\gamma = 3.5$, $\alpha_1 = 0.2$ and $\alpha_2 = 0.8$.

to force the dynamics of the activator. Numerical simulations using Oregonator type models have been used to reproduce these experimental findings[11,12,19]. In this paper, we have studied the underlying dynamic mechanisms that lead to phase-locked and localized oscillatory patterns in a two-cluster system of globally coupled Oregonators capturing the experimental results mentioned above. Our mechanistic study contributes to both the understanding of the conditions under which these cluster patterns occur and to the elucidation of the role played by the participating chemicals and reaction rate constants through the model parameters η, ϵ, and q.

Our approach consisted of assuming that a large system of globally coupled chemical

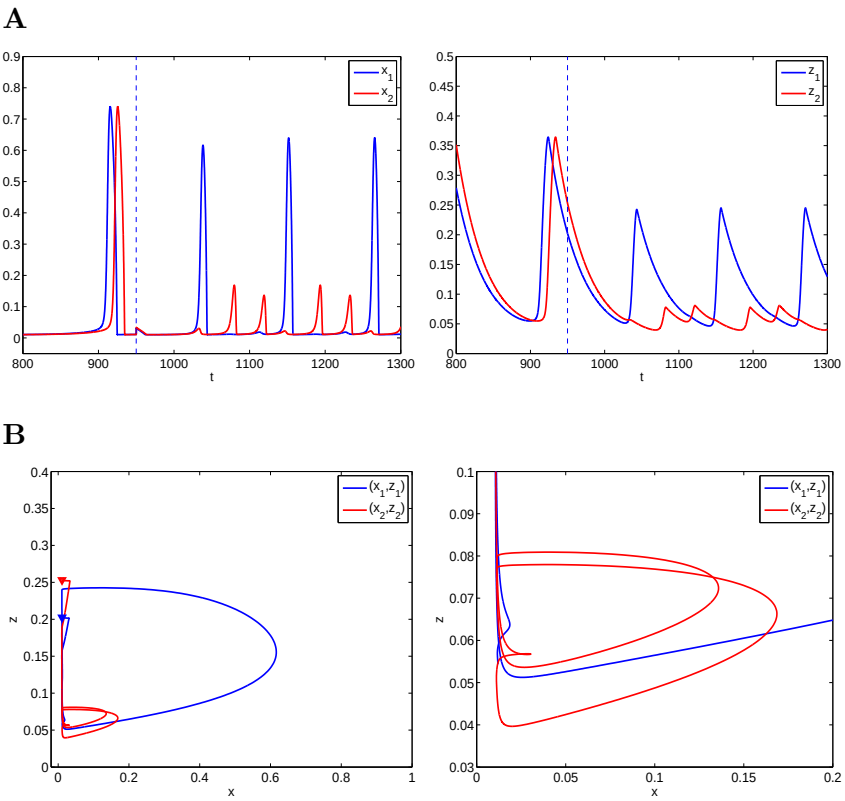

FIG. 14. **Dynamics of the globally coupled Oregonator model for a representative set of parameters. A.** x- and z-traces. The vertical dashed-lines indicate the time at which global coupling is activated. (For lower values of t the system is uncoupled.) **B.** Trajectories in phase-space projected onto the (x_1, z_1)-plane (left) (x_2, z_2)-plane (right). The arrows indicate both the connection time and the direction of motion of the trajectory at the connection time. We used the following parameters: $\eta = 2$, $\epsilon = 0.025$, $q = 0.01$, $\gamma = 5$, $\alpha_1 = 0.2$ and $\alpha_2 = 0.8$.

oscillators is initially organized into two clusters. All elements in a given cluster are identical; i.e., they oscillate with the same phase and amplitude. Differences in cluster sizes translate into weights (σ_1 and σ_2) in the global coupling term. We investigated the circumstances under which a two-cluster system with an initially small phase evolves into steady phase-locked or localized two-cluster patterns, and how the phase and amplitudes of these patterns depend on the model parameters.

We found that for large enough values of the stoichiometric parameter η, the canard-related, swing-and-release mechanism is responsible for the fast phase separation leading to antiphase patterns. The stabilization of these patterns is achieved by a combination

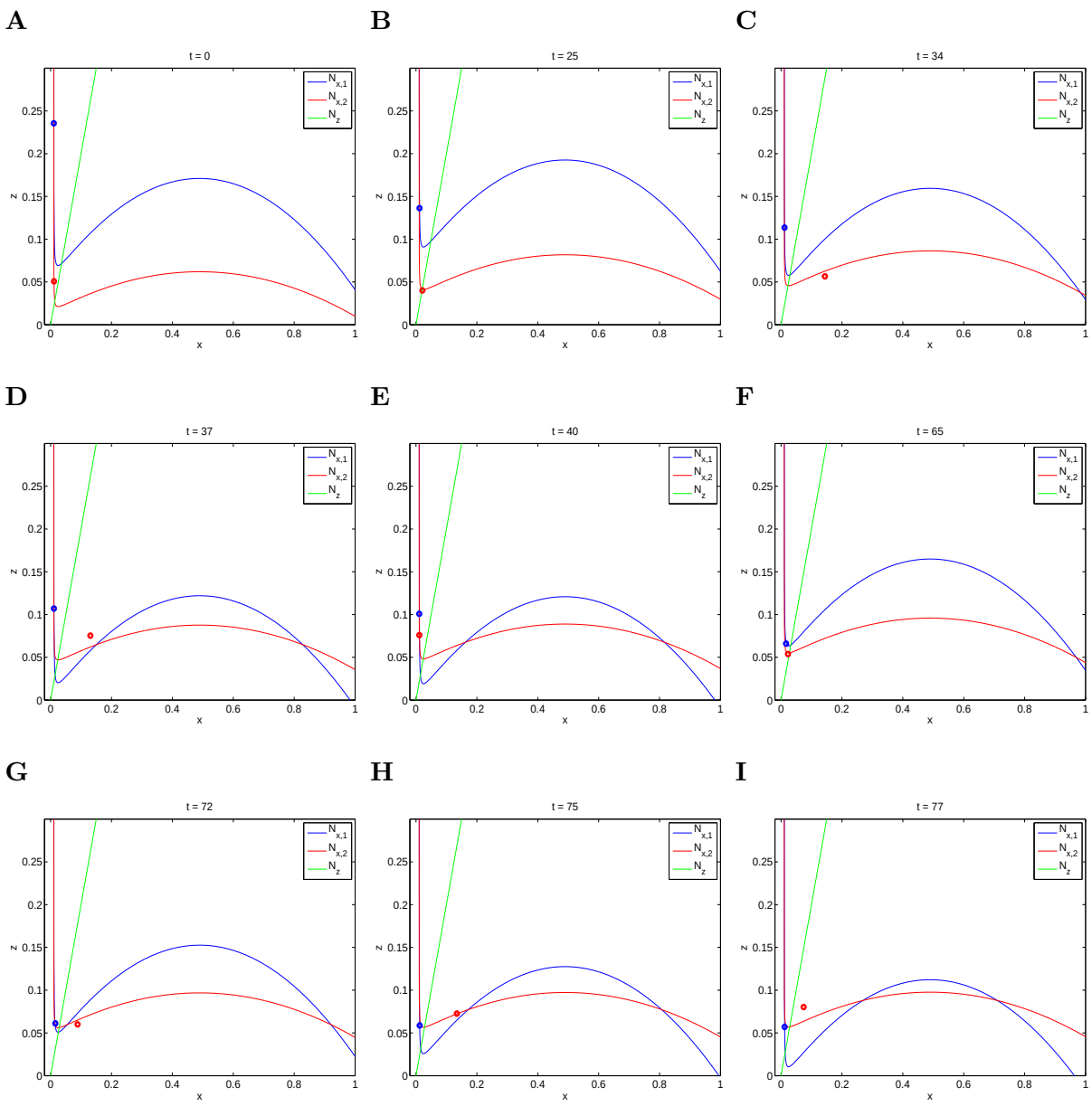

FIG. 15. **Globally coupled Oregonator (part I).** Snapshots of the phase-plane for the two globally coupled oscillators for representative values of t. We used the following parameters: $\eta = 2$, $\epsilon = 0.025$, $q = 0.01$, $\gamma = 5$, $\alpha_1 = 0.2$ and $\alpha_2 = 0.8$. This figures continues in Fig. 16.

of the hold-and-release and hold-and-escape mechanisms. This persists for smaller values of η, provided the value of the global feedback parameter γ is large enough; however, for smaller values of γ, phase separation occurs at a slower pace by a combination of the hold-and-release and hold-and-escape mechanisms. These mechanisms have been identified in[18] for the globally coupled FHN model and are related to the synaptic release and escape

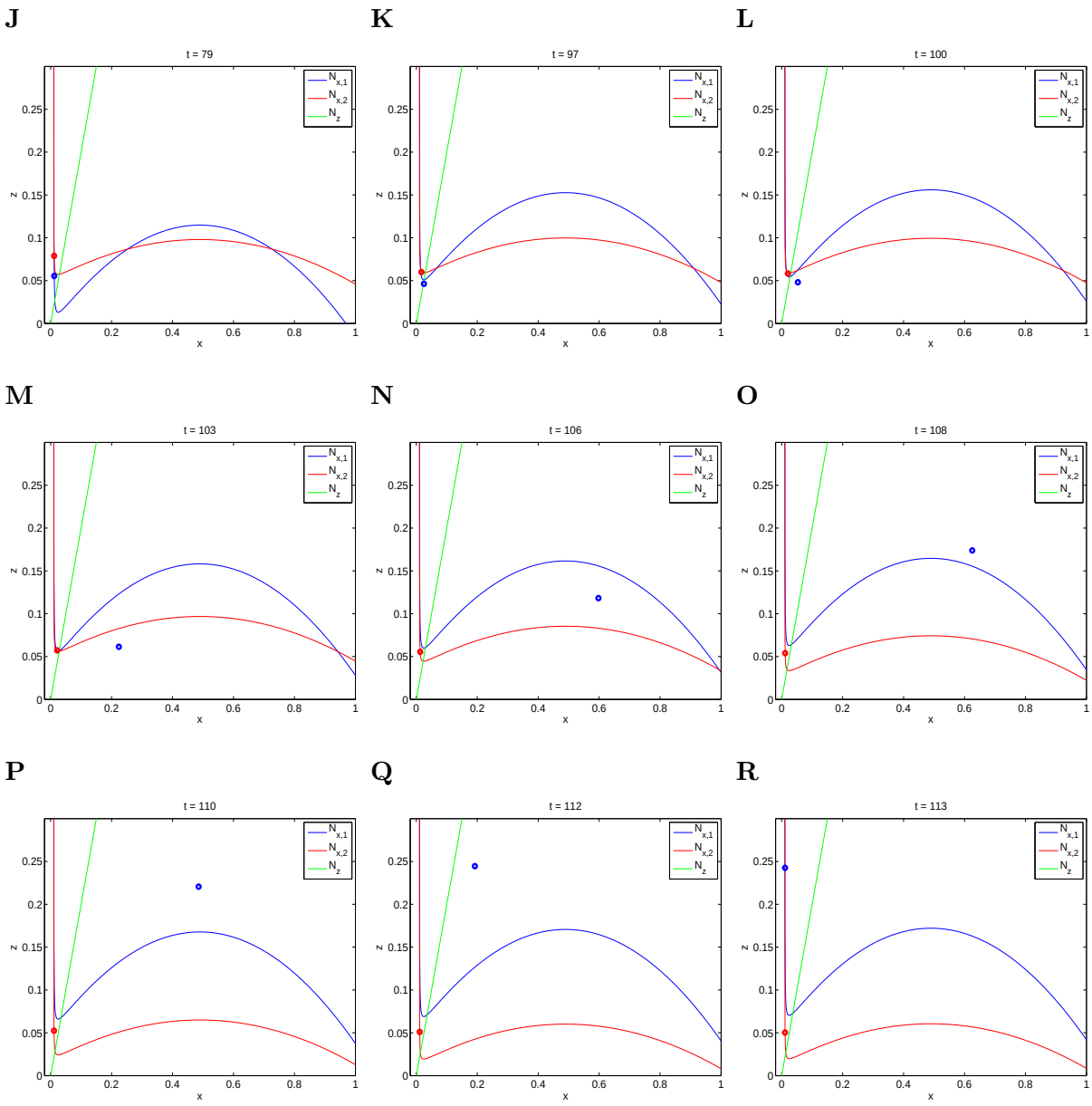

FIG. 16. **Globally coupled Oregonator (part II).** Snapshots of the phase-plane for the two globally coupled oscillators for representative values of t. We used the following parameters: $\eta = 2$, $\epsilon = 0.025$, $q = 0.01$, $\gamma = 5$, $\alpha_1 = 0.2$ and $\alpha_2 = 0.8$. This figure is the continuation of Fig. 15

mechanisms described for synaptically connected neurons[33].

Homogeneous clusters ($\sigma_1 = \sigma_2$) display only phase-locked (antiphase) patterns. (When two clusters synchronize in-phase they are considered as a single cluster.) Heterogeneous clusters ($\sigma_1 \neq \sigma_2$) display both phase-locked and localized patterns where the oscillation amplitude of the largest cluster is roughly an order of magnitude smaller than the oscillation

amplitude of the smaller cluster. The transition from phase-locked to localized cluster patterns occurs as γ increases, and is less abrupt (more diffuse) than the transition observed for the globally coupled modified Oregonator[17]. As for the latter, localized patterns in the globally coupled Oregonator studied here are generated by a canard mechanism. Consistent with this, SAOs are displayed by the largest cluster rather than by the smallest one, reflecting a self-inhibition effect that increases with cluster size as the activator (cubic-like) nullcline of the largest cluster becomes flatter.

The globally coupled Oregonator model studied here has similarities and differences with the globally coupled FHN system studied in[18]. In both models the inhibitor nullcline is linear and the global coupling term is of the same type (the activator receives global feedback from the inhibitor). Conversely to the FHN model, where the activator nullcline is "purely cubic" and all three branches become flatter as γ increases, the activator nullcline in the Oregonator has an almost vertical left branch that does not significantly change with increasing values of γ. In addition, the global coupling term in the Oregonator is nonlinear in the activator variable while it is linear in both the activator and inhibitor variables in the FHN model. The differences between these two modes result in different type of patterns for certain parameter values. Most notably, the globally coupled Oregonator supports localized solutions that we have not observed in the globally coupled FHN model, and the FHN model supports M:1 oscillations with roughly the same amplitude that are more rare in the globally coupled Oregonator. In fact, one could think of the localized solutions as M:1 patterns where the "M oscillations" have small amplitude rather than large amplitude.

In this paper we have not investigated the effects of changes in the parameters q and ϵ which were assumed to be fixed. The parameter ϵ represents the time scale separation between the activator and inhibitor. The canard-related swing-and-release mechanism is strongly dependent on the fact that the system is fast-slow ($0 < \epsilon \ll 1$). Our conclusions are expected to hold for some larger range of values of ϵ than the one considered here. The type of patterns obtained for values of ϵ outside this regime and the mechanisms that give rise to these patterns call for more research. The value of the parameter q is responsible for the strong nonlinearity (almost vertical left branch) mentioned in the previous paragraph.

Globally coupled oscillatory systems have been studied both experimentally and theoretically in chemical, biochemical, biological and neural systems[11,12,16,17,19,36,52–64]. The results presented in this paper and the methods we and other authors have developed[18,31,32,65,66] can

be applicable to the understanding of the underlying mechanisms that govern the dynamics in these systems.

In this paper, we focused on the mechanisms of generation of two-cluster patterns by assuming the set of individual oscillators is initially divided into two clusters oscillating out-of-phase but not on the mechanism by which these individual oscillators are grouped into clusters. More research is needed to understand these mechanisms and to determine how the selection of cluster sizes depends on the model parameters and how individual oscillators are spatially grouped into clusters in systems including diffusion.

Acknowledgments

The authors are grateful to David Fox for reading this manuscript. This work was supported by the National Science Foundation grant DMS-0817241 (HGR).

Appendix A: Canard critical value for the uncoupled Oregonator

The fixed point $(\bar{x}, \bar{z})$ for system (4) is given by

$$\bar{x} = \frac{1 - \eta - q + \sqrt{(1-\eta-q)^2 + 4\,q\,(\eta+1)}}{2} \qquad \text{and} \qquad \bar{z} = \eta\,\bar{x}. \tag{A1}$$

The minimum (x_m, z_m) of the x-nullcline $N_x(x)$ in (5) is given by the middle root of the following polynomial

$$2\,x^3 - (2\,q+1)\,x^2 - 2\,q\,(q-1)\,x + q^2 = 0. \tag{A2}$$

For $q \ll 1$, the largest root is $\sim 1/2$ and the smallest root is negative. Call

$$\lambda = \frac{1}{\eta}$$

The value of λ corresponding to the intersection between the two nullclines at the point (x_m, z_m) is given by

$$\lambda_m = \frac{x_m}{z_m}$$

The canard critical value is given by[67]

$$\eta_{cr} = \frac{1}{\lambda_m + \lambda_c} \tag{A3}$$

with

$$\lambda_c(\sqrt{\epsilon}) = -\frac{G_x}{2\,F_{xx}^3\,|G_\lambda|}[\,G_x\,F_{xz}\,F_{xx} + G_x\,|F_z|\,F_{xxx} - |F_z|\,G_{xx}\,F_{xx} + G_z\,F_{xx}^2\,]\,\epsilon + \mathcal{O}(\epsilon^{3/2}), \tag{A4}$$

where

$$F(x,z) = x\,(1-x) + \frac{q-x}{q+x}\,z, \qquad G(x,z,\lambda) = \frac{x}{\lambda} - z,$$

and all the functions are calculated at the point (x_m, z_m) and $\lambda = \lambda_m$.

REFERENCES

[1]F. Sagués and I. R. Epstein, "Nonlinear chemical dynamics," Dalton Trans., 1201–1217(2003).

[2]J. D. Murray, *Mathematical Biology* (Springer, Berlin, 1989).

[3]S. H. Strogatz, *Nonlinear Dynamics and Chaos* (Addison Wesley, Reading MA, 1994).

[4]B. P. Belousov, "A periodic reaction and its mechanism," Compilation of Abstracts on Radiation Medicine (Med. Publ., Moscow) **147**, 145 (1959).

[5]B. P. Belousov, "A periodic reaction and its mechanism," in Field, R. J. and Burger, M., Eds., Oscillations and traveling waves in chemical systems (Wiley, New York)(1985).

[6]A. M. Zhabotinksy, "Periodic processes of malonic acid oxidation in a liquid phase," Biofizika **9**, 306–311 (1964).

[7]A. M. Zhabotinksy, "Belousov-Zhabotinsky reaction," Scholarpedia **2**, 1435 (2007).

[8]Other chemical species involved are potassium bromate ($KBrO_3$), potassium bromide (KBr), and sulfuric acid (H_2SO_4).

[9]$(phen) = 1,10 - Phenanthroline$.

[10]The reaction occurs in various steps: (1) $HBrO_2$ is involved into an autocatalytic reaction (explosion process). Ferriin (oxidized form or ferroin) is produced. (2) The concentration of ferriin becomes large, interacts with organic components, and starts to slowly change back to ferroin. Bromide (Br^-) is produced. (3) Bromide is an effective inhibitor of the autocatalytic process so the production of $HBrO_2$ is stopped and its amount reduced. (4) Br^- are binded (concentration reduced) and the system is able to repeat step (1).

[11]V. K. Vanag, L. Yang, M. Dolnik, A. M. Zhabotinsky, and I. R. Epstein, "Oscillatory cluster patterns in a homogeneous chemical system with global feedback," Nature **406:(6794)**, 389–391 (2000).

[12]V. K. Vanag, A. M. Zhabotinsky, and I. R. Epstein, "Pattern formation in the Belusov-Zhabotinsky reaction with photochemical global feedback," J. Phys. Chem. A **104**, 11566–11577 (2000).

[13](bipy) = 2,2'-bipyridine.

[14]D. Golomb and J. Rinzel, "Clustering in globally coupled inhibitory neurons," Physica D **72**, 259–282 (1994).

[15]D. Golomb, D. Hansel, B. Shraiman, and H. Sompolinksy, "Clustering in globally coupled

phase oscillators," Phys. Rev. A **45**, 3516–3530 (1992).

[16]H. G. Rotstein, N. Kopell, A. Zhabotinsky, and I. R. Epstein, "A canard mechanism for localization in systems of globally coupled oscillators," SIAM J. Appl. Math. **63**, 1998–2019 (2003).

[17]H. G. Rotstein, N. Kopell, A. Zhabotinsky, and I. R. Epstein, "Canard phenomenon and localization of oscillations in the Belousov-Zhabotinsky reaction with global feedback," J. Chem. Phys **119 (17)**, 8824–8832 (2003).

[18]H. G. Rotstein and H. Wu, "Swing, release, and escape mechanisms contribute to the generation of phase-locked cluster paterns in a globally coupled fitzhugh-nagumo model," submitted(2012).

[19]L. Yang, M. Dolnik, A. M. Zhabotinsky, and I. R. Epstein, "Oscillatory clusters in a model of the photosensitive Belusov-Zhabotinsky reaction system with global feedback," Phys. Rev. E **62(5)**, 6414–6420 (2000).

[20]R. J. Fields, E. Koros, and R. M. Noyes, "Oscillations in chemical systems. 2. thorough analysis of temporal oscillation in bromate-cerium-malonic acid system," J. Am. Chem. Soc. **94**, 8649–8664 (1972).

[21]R. J. Field and M. Burger, *Oscillations and traveling waves in chemical systems* (John Wiley & sons, 1985).

[22]I. R. Epstein and K. Showalter, "Nonlinear chemical dynamics: Oscillations, patterns and chaos," J. Phys. Chem. **100**, 13132–13147 (1996).

[23]I. R. Epstein and J. A. Pojman, *An introduction to nonlinear chemical dynamics* (Oxford University Press, 1998).

[24]A. M. Zhabotinsky, F. Buchholtz, A. B. Kiyatkin, and I. R. Epstein, "Oscillations and waves in metal-ion-catalyzed bromate oscillating reactions in highly oxidized states," J. Phys. Chem. **97**, 7578–7584 (1993).

[25]R. FitzHugh, "Impulses and physiological states in models of nerve membrane," Biophysical J. **1**, 445–466 (1961).

[26]J. S. Nagumo, S. Arimoto, and S. Yoshizawa, "An active pulse transmission line simulating nerve axon," Proc. IRE **50**, 2061–2070 (1962).

[27]J. Keener and J. Sneyd, *Mathematical Physiology* (Springer-Verlag, New York, 2001).

[28]H. G. Rotstein and H. Wu, "Swing, release, and escape mechanisms contribute to the generation of phase-locked cluster paterns in a globally coupled fitzhugh-nagumo model,"

NJIT CAMS Technical Reports **1112-9**, 1–37 (2012).

[29]W. Eckhaus, "Relaxation oscillations including a standard chase on French ducks," In Lecture Notes in Mathematics, Springer-Verlag **985**, 449–497 (1983).

[30]M. Krupa and P. Szmolyan, "Extending geometric singular perturbation theory to nonhyperbolic points - fold and canard points in two dimensions," SIAM J. Math. Anal. **33(2)**, 286–314 (2001).

[31]X.-J. Wang and J. Rinzel, "Alternating and synchronous rhythms in reciprocally inhibitory model neurons," Neural Computation **4**, 84–97 (1992).

[32]F. K. Skinner, N. Kopell, and E. Marder, "Mechanisms for oscillations and frequency control in networks of mutually inhibitory relaxation oscillators," Journal of Computational Neuroscience **69-87** (1994).

[33]N. Kopell and G. B. Ermentrout, "Mechanisms of phase-locking and frequency control in pairs of coupled neural oscillators," In Handbook on Dynamical Systems: Toward applications. Ed. B. Fiedler, Elsevier **2**, 3–54 (2002).

[34]J. J. Tyson, "Oscillations, bistability and echo waves in models of the Belousov-Zhabotinskii reaction," Ann. New York Acad. Sci. **316**, 279 (1979).

[35]M. Somani, M. A. Liwuw, and D. Luss, "Evolution and impact of temperature patterns during hydrogen oxidation on a Ni ring," Chem. Engg. Sci. **52**, 2331 (1997).

[36]A. Birzu and K. Krischer, "Resonance tongues in a system of globally coupled oscillators with time-periodic coupling strength," Chaos **20**, 043114 (2010).

[37]F. Dumortier and R. Roussarie, "Canard cycles and center manifolds," Memoirs of the American Mathematical Society **121 (577)**, 1–100 (1996).

[38]S. M. Baer and T. Erneux, "Singular Hopf bifurcation to relaxation oscillations," SIAM J. Appl. Math. **52**, 1651–1664 (1992).

[39]E. Benoit, J. L. Callot, F Diener, and Diener M., *Chasse au Canard*, Vol. 31 (Collect. Math., 1981) pp. 37–119.

[40]M. Krupa and P. Szmolyan, "Relaxation oscillation and canard explosion," J. Diff. Eq. **174**, 312–368 (2001).

[41]F. Dumortier, "Techniques in the theory of local bifurcations: Blow-up, normal forms, nilpotent bifurcations, singular perturbations," In Bifurcations and Periodic Orbits of Vector Fields, edited by D. Schlomiuk (Kluwer Academic Press, Dordrecht), 19–73(1993).

[42]H. G. Rotstein, S. Coombes, and A. M. Gheorghe, "Canard-like explosion of limit cycles in

two-dimensional piecewise-linear models of FitzHugh-Nagumo type," SIAM J. Appl. Dyn. Systems **11**, 135–180 (2012).

[43]M. Wechselberger, "Existence and bifurcation of canards in R^3 in the case of a folded node," SIAM J. Appl. Dyn. Syst. **4**, 101–139 (2005).

[44]M. Brøns, M. Krupa, and M. Wechselberger, "Mixed mode oscillations due to the generalized canard phenomenon," in Fields Institute Communications Bifurcation theory and spatio-temporal pattern formation, Wayne Nagata, N. Sri Namachchivaya (Eds.) **49**, 39–63 (2006).

[45]A. Milik and P. Szmolyan, "Multiple time scales and canards in a chemical oscillator," in Multiple Time-Scale Dynamical systems (IMA Volume) edited by C. K. R. T. Jones and A. Khibnik (Springer - New York) **122**, 117–140 (2000).

[46]F. Buchholtz, M. Dolnik, and I. R. Epstein, "Diffusion-induced instabilities near a canard," J. Phys. Chem. **99**, 15093–15101 (1995).

[47]M. Brøns and K. Bar-Eli, "Canard explosion and excitacion in a model of the Belousov-Zabotinsky reaction," J. Phys. Chem. **95**, 8706–8713 (1991).

[48]K. Bar-Eli and M. J. Brøns, "Period lengthening near the end of oscillations in chemical systems," J. Phys. Chem. **94**, 7170–7177 (1990).

[49]A. Milik, P. Szmolyan, H. Löffelmann, and E. Groller, "Geometry of mixed-mode oscillations in the 3D-autocatalator," Int. J. Bif. Chaos **8**, 505–519 (1998).

[50]J. Moehlis, "Canards in a surface oxidation reaction," J. Nonlinear Sci. **12**, 319–345 (2002).

[51]H. G. Rotstein and R. Kuske, "Localized and asynchronous patterns via canards in coupled calcium oscillators," Physica D **215**, 46–61 (2006).

[52]R. Toth, A. F. Taylor, and M. R. Tinsley, "Collective behavior of a population of chemically coupled oscillators," J. Phys. Chem. B **110**, 10170–10176 (2006).

[53]A. F. Taylor, M. R. Tinsley, F. Wang, Z. Huang, and K. Showalter, "Dynanical quorum sensing and synchronization in large populations of chemical oscillators," Science **323**, 614–617 (2009).

[54]D. Gonze, N. Markadieu, and A. Goldbeter, "Selection of in-phase or out-of-phase synchronization in a model based on global coupling of cells undergoing metabolic oscillations," Chaos **18**, 037127 (2008).

[55]A. F. Taylor, P. Kapetanopoulos, B. J. Whitaker, R. Toth, L. Bull, and M. R. Tinsley, "Phase clustering in globally coupled photochemical oscillators," Eur. Phys. J. Special

Topics **165**, 137–149 (2008).

[56]M. Bertram, C. Beta, M. Pollmann, A. S. Mikhailov, H. H. Rotermund, and G. Ertl, "Pattern formation on the edge of chaos: Experiments with CO oxidation on a Pt(110) surface under global delayed feedback," Phys. Rev. E **67**, 036208 (2003).

[57]Kim M., M. Bertram, M. Pollmann, A. von Oertzen, A. S. Mikhailov, H. H. Rotermund, and G. Ertl, "Controlling chemical turbulence by global delayed feedback: Pattern formation in catalytic CO oxidation on Pt(110)," Science **292**, 1357–1360 (2001).

[58]F. Plenge, P. Rodin, E. Schöll, and K. Krischer, "Breathing current domains in globally coupled electrochemical systems: A comparison with a semiconductor model," Phys. Rev. E **64**, 056229 (2001).

[59]M. A. Liauw, P. J. Plath, and N. I. Jaeger, "Complex oscillations and global coupling during the catalytic oxidation of CO," J. Chem. Phys **104**, 6375–6386 (1996).

[60]R. A. Stefanescu and V. K. Jirsa, "A low dimensional description of globally coupled heterogeneous neural networks of excitatory and inhibitory neurons," PLoS Computational Biology **4**, e1000219 (2008).

[61]E. Alvarez-Lacalle and B. Echebarria, "Global coupling in excitable media provides a simplified description of mechanoelectrical feedback in cardiac tissue," Phys. Rev. E **79**, 031921 (2009).

[62]K. Miyakawa and K. Yamada, "Synchronization and clustering in globally coupled salt-water oscillators," Physica D **151**, 217–227 (2001).

[63]A. Koseska, E. Volkov, A. Zaikin, and J. Kurths, "Inherent multistability in arrays of autoinducer coupled genetic oscillators," Phys. Rev. E **75**, 031916 (2007).

[64]A. Koseska, E. Volkov, and J. Kurths, "Detuning-dependent dominance of oscillation death in globally coupled synthetic genetic oscillators," Europhysics Letters **85**, 28002 (2009).

[65]G. B. Ermentrout and D. Terman, *Mathematical Foundations of Neuroscience* (Springer, 2010).

[66]J. Rubin and D. Terman, "Analysis of clustered firing patterns in synaptically coupled networks of oscillators," J. Math. Biol. **41**, 513–545 (2000).

[67]H. G. Rotstein, S. Coombes, and A. M. Gheorghe, "Canard-like explosion of limit cycles in two-dimensional piecewise-linear models of FitzHugh-Nagumo type," NJIT CAMS Technical Report **1112-4**, 1–60 (2011).